

Photoionization of Rb^{2+} ions in the valence energy region 37 eV – 44 eV

Brendan M McLaughlin^{1,2†} and James F Babb^{2‡}

¹Centre for Theoretical Atomic, Molecular and Optical Physics, School of Mathematics and Physics, The Old Physics Building, Queen's University Belfast, Belfast BT7 1NN, UK

²Institute for Theoretical Atomic and Molecular Physics, Center for Astrophysics, Harvard & Smithsonian, Cambridge, MA 02138, USA

Abstract. Absolute photoionization cross sections for the Rb^{2+} ion were recently measured at high resolution over the energy range 37.31 eV – 44.08 eV, with autoionizing Rydberg resonance series identified, using the photon-ion merged-beam setup at the Advanced Light Source (ALS) in Berkeley (Macaluso D A et. al. *J. Phys. B: At. Mol. Opt. Phys.* **49** (2016) 235002; **50** (2017) 119501). Detailed photon-energy scans taken at 13.5 ± 2.5 meV bandwidth illustrated multiple Rydberg resonance series associated with the ground and metastable states. Here we present theoretical cross section results obtained using the Dirac-Coulomb R -matrix approximation with a detailed analysis of the resonances. The calculations were performed for the $3d^{10}4s^24p^5\ ^2P^{\circ}_J$, $J = \frac{3}{2}$ ground state and the corresponding $3d^{10}4s^24p^5\ ^2P^{\circ}_J$, $J = \frac{1}{2}$ metastable level. Results from the large-scale calculations are benchmarked against the ALS high-resolution measurements and reproduce the dominant resonance features in the spectra, providing confidence in the theoretical work for astrophysical applications.

PACS numbers: 32.80.Fb, 31.15.Ar, 32.80.Hd, and 32.70.-n

Short title: Photoionization of the atomic rubidium ion Rb^{2+}

Submitted to: *J. Phys. B: At. Mol. Opt. Phys.* : 3 March 2022

† Corresponding author, E-mail: bmclaughlin899@btinternet.com

‡ Corresponding author, E-mail: jbabb@cfa.harvard.edu

1. Introduction

Photoionization of atomic ions is an important process in determining the ionization balances and the abundances of elements in photoionized astrophysical nebulae. It has recently become possible to detect neutron-capture elements (Se, Cd, Ga, Ge, Rb, Kr, Br, Xe, Ba, Pb, etc.) in ionized nebulae [1–6]. These elements are produced by slow (*s*-process) or rapid (*r*-process) neutron-capture nucleosynthesis. Measuring the abundances of these elements helps to reveal their dominant production sites in the Universe, as well as details of stellar structure, mixing and nucleosynthesis [2, 6, 7], but abundance determinations are affected by a lack of atomic data [8–10]. In addition to what can be learned from planetary nebulae, Walker *et al.* [11] used observations of the interstellar $^{85}\text{Rb}/^{87}\text{Rb}$ abundance ratio to gain insight into the relative roles of various *n*-capture processes in massive stars. Such astrophysical observations are the motivation to determine the electron-impact excitation (EIE), electron-impact ionisation (EII), photoionization (PI), and recombination properties of neutron-capture elements [7, 12–18].

With respect to Rb, specifically in support of astrophysical applications, recent work includes calculations of 538 transition energies, transition probabilities, and oscillator strengths of Rb^{3+} , substantially adding to the known data [19, 20], and calculations of transition probabilities and collision strengths for 10 forbidden transitions originating in the ground state of Rb^{3+} [6]. In addition, photoionization cross sections of Rb^+ were measured [21–23] and calculated [24, 25].

The motivation for the present study of the *trans*-Fe element Rb^{2+} is to provide benchmark PI cross section data for applications in astrophysics, to aid in the formulation of so-called “ionization correction factors” used in the modeling of planetary nebular emission lines of ions of Rb [6, 10, 26]. High-resolution measurements of the photoionization cross section for Rb^{2+} with experimentally resolved Auger Rydberg resonance series were recently published in the literature [27, 28]. These high-resolution measurements, made over the photon energy range 37.31 – 44.08 eV at the ALS synchrotron radiation facility in Berkeley, California, were taken with a band pass resolution of 13.5 ± 2.5 meV full width half maximum (FWHM). In tandem with the experiment, *R*-matrix calculations were performed in the intermediate coupling *jK* Breit-Pauli approximation facilitating the identification of several highly excited Auger Rydberg resonance states.

In the present investigation we use a fully relativistic approach within the Dirac-Coulomb *R*-matrix approximation to calculate the cross sections for ground and metastable states. The high resolution ALS photoionization cross sections are used to benchmark the present PI cross sections and Auger Rydberg resonances. Excellent agreement is found, providing confidence in our theoretical data for various astrophysical applications.

This paper is structured as follows: Section 2 presents a brief outline of the theoretical work that was carried out. Section 3 presents comparisons of the calculated PI cross sections and Rydberg resonance series with the experimental data. In section 4 we present a discussion of these results. Finally in section 5, conclusions are drawn from the present investigation.

2. Theory

High-resolution PI cross-section measurements require state-of-the-art theoretical methods with relativistic effects [29–31], in order to obtain suitable agreement with experiment. The present work employs an efficient parallel version [32,33] of the Dirac-Atomic R -matrix-Codes (DARC) [34–38] developed for treating electron and photon interactions with atomic systems. This suite continues to evolve [39–44] in order to address ever increasing expansions for the target and collision models used in electron and photon impact with heavy atomic systems [45,46]. The latest example of the application to photoionization is the recent comparison of experiment and theory for the Ca^+ [47] and Rb^+ [24] ions and the theoretical work on neutral Fe [48]. Suitable agreement of the DARC photoionization cross-sections with high resolution measurements performed at leading synchrotron light sources was obtained.

2.1. Atomic structure

The GRASP code [29–31] was used to generate the residual Rb^{3+} target wave functions employed in our collision work. All orbitals were physical up to $n = 3$, and in addition the $4s$, $4p$, $4d$, $5s$, $5p$ and $5d$ orbitals were included. We began by performing an extended averaged level (EAL) calculation for the $n = 4$ orbitals and extended these calculations with the addition of the $n = 5$ orbitals. All EAL calculations were performed on the lowest 18 fine-structure levels of the residual Rb^{3+} ion in order to generate target wave functions for our photoionization studies. In our work we retained all the 687 - levels originating from one, and two-electron promotions from the $n = 4$ levels into the orbital space of this ion. All 687 levels arising from the sixteen configurations were included in the DARC close-coupling calculation, namely, the one-electron promotions, $3d^{10}4s^24p^4$, $3d^{10}4s4p^5$, $3d^{10}4s4p^44d$, $3d^{10}4s4p^45s$, $3d^{10}4s4p^45p$, $3d^{10}4s4p^45d$, $3d^{10}4s^24p^34d$, $3d^{10}4s^24p^35s$, $3d^{10}4s^24p^35p$ and $3d^{10}4s^24p^35d$. In addition we include the two-electron promotions, $3d^{10}4s^24p^24d^2$, $3d^{10}4s^24p^25s^2$, $3d^{10}4s^24p^25p^2$, $3d^{10}4s^24p^25d^2$, $3d^{10}4p^44d^2$, and $3d^{10}4p^45s^2$. This provides a suitable representation of the residual Rb^{3+} ionic levels, as shown in Table 1, where the energies of the lowest 9 levels of the residual Rb^{3+} ion from the 687-level GRASP calculations are compared to the values from the NIST tabulations [49] and from the ALS measurements [27]. We note that the average percentage difference of our theoretical energy levels compared with the NIST values is approximately 7%.

Photoionization cross section calculations were performed for the Rb^{2+} ion in the $3d^{10}4s^24p^5\ ^2\text{P}^{\circ}_{3/2}$ ground state and in the $3d^{10}4s^24p^5\ ^2\text{P}^{\circ}_{1/2}$ metastable level using the DARC codes with the above Rb^{3+} residual ion target wave functions.

2.2. Photoionization

In our work we used sixteen continuum basis functions and a boundary radius of 14.65 Bohr to accommodate all the diffuse $n = 5$ orbitals. This resulted in Hamiltonian and dipole matrix sizes in excess of 45,000 with over 3,000 coupled channels in our close coupling calculations. For the ground and metastable initial states of the rubidium ions studied here, the outer region electron-ion collision problem was solved (in the resonance region below and between all thresholds) using an extremely fine energy mesh of 5×10^{-8} Rydbergs ($\approx 0.680\ \mu\text{eV}$) for the excited levels investigated. The jj -coupled Hamiltonian diagonal matrices energies were shifted so that the theoretical term energies matched the recommended NIST values [49]. We note that this energy

Table 1. Comparison of Rb^{3+} energy levels from the GRASP code (present work) with NIST tabulations [49] and ALS measurements [27]. Energies are with respect to the ground state and given in eV. Percentage differences $\Delta(\%)$ are included for completeness.

Level	Configuration	Term	J	NIST Energy [†] (eV)	GRASP Energy ^a (eV)	ALS Energy ^b (eV)	Δ_1^c (%)	Δ_2^d (%)
1	$3d^{10}4s^24p^4$	3P	2	0.000000	0	0	0.0	0.0
2			1	0.776188	0.753086	0.776 ± 0.010	-3.1	-3.0
3			0	0.861415	0.897535	–	3.9	–
4	$3d^{10}4s^24p^4$	1D	2	2.152076	2.418777	2.152 ± 0.010	12.4	12.4
5	$3d^{10}4s^24p^4$	1S	0	4.761436	6.016326	4.771 ± 0.010	26.4	26.1
6	$3d^{10}4s4p^5$	$^3P^o$	2	16.735202	17.660408	–	5.5	–
7			1	17.310417	18.245856	–	5.4	–
8			0	17.681250	18.610682	–	5.3	–
9	$3d^{10}4s4p^5$	$^1P^o$	1	20.831188	22.187881	–	6.5	–

[†]NIST Atomic Spectra Database tabulations [49].

^aPresent GRASP theoretical energies.

^bALS experimental analysis [27].

^c $\Delta_1(\%)$ the percentage difference between the GRASP and NIST [49] experimental values.

^d $\Delta_2(\%)$ the percentage difference between the GRASP and ALS [27] experimental values.

adjustment ensures better positioning of resonances relative to all thresholds included in the calculation [37, 38].

In the present work the DARC PI cross-section calculations were convolved with a Gaussian distribution function to simulate the experimental photon energy bandwidth. Mathematically, a convolution is defined as the integral \mathcal{I} over all space of the product of a function $F(x)$ and a function $G(u - x)$,

$$\mathcal{I}(u) = \int F(x)G(u - x)dx. \quad (1)$$

The integration is taken over the variable x (which may be a 1D or 3D variable), typically from minus infinity to infinity over all the dimensions. In the present work the integration energy range for the convolution of the theoretical PI cross sections is that of the Rb^{2+} experimental spectrum, F is the numerical theoretical cross section as a function of the photon energy and G will be the Gaussian distribution [50] corresponding to the resolution of the experimental measurements. Fig 1 gives a comparison of the theoretical PI cross section from the 687-level DARC calculations with the ALS measurements. In order to compare directly with experiment we have statistically averaged over the ground and metastable initial states and convolved our cross sections with a Gaussian distribution having a profile of 13.5 meV. The statistical averaged cross section σ^{Total} as a function of energy E is

$$\sigma^{\text{Total}}(E) = \frac{1}{3}\sigma(^2P_{1/2}^o) + \frac{2}{3}\sigma(^2P_{3/2}^o), \quad (2)$$

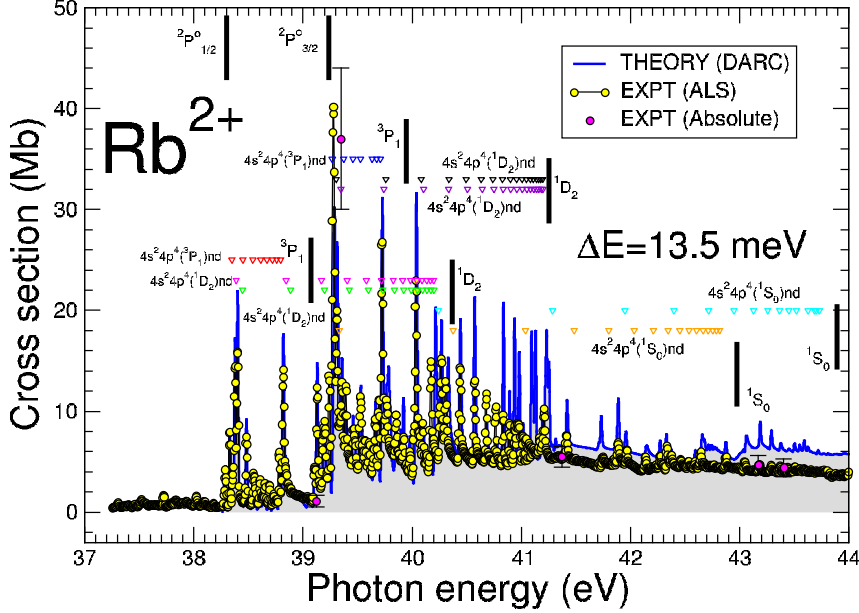


Figure 1. (Colour online) Single photoionization cross section of Rb^{2+} in the energy region 37 - 44 eV. Experimental measurements (solid yellow circles) on an absolute scale with the absolute cross section measurements (solid magenta circles) made at selected energies used to normalized the photo-ion yield spectra. See the work of Macaluso and co-workers for further details [27, 28]. Cross section results from the merged beam measurements at the ALS radiation facility, obtained at a photon energy resolution of 13.5 ± 2.5 meV FWHM, are compared with those from an 687-level Dirac R -matrix (DARC) approximation. The DARC photoionization cross sections (solid blue line) were convolved with a Gaussian distribution having a 13.5 meV FWHM profile and statistically averaged for the ground state $3d^{10}4s^2 4p^5 \ ^2P_{3/2}^{\circ}$ and $3d^{10}4s^2 4p^5 \ ^2P_{1/2}^{\circ}$ metastable state (see text for details). The inverted triangles are the energy positions of the various $4s^2 4p^4 nd$ Rydberg resonance series found in the Rb^{2+} photoionization spectrum, originating from the $^2P_{1/2}^{\circ}$ and $^2P_{3/2}^{\circ}$ initial states, for the energy region investigated. The solid black vertical lines indicate the photon energies required to ionize the $Rb^{2+} \ ^2P_{1/2}^{\circ}$ and $^2P_{3/2}^{\circ}$ states and the limits for the each of the $4s^2 4p^4 nd$ Rydberg series converging to 3P_1 , 1D_2 , or 1S_0 states of the residual Rb^{3+} ion.

with, respectively, $\sigma(^2P_{3/2}^{\circ})$ and $\sigma(^2P_{1/2}^{\circ})$ the photoionization cross sections for the ground and metastable states. Over the entire photon energy range investigated the theoretical results from the 687-level DARC calculations are in good agreement with the high resolution ALS measurements. As illustrated in Fig 1, multiple Rydberg resonance series are seen in the cross sections. We now discuss their analysis.

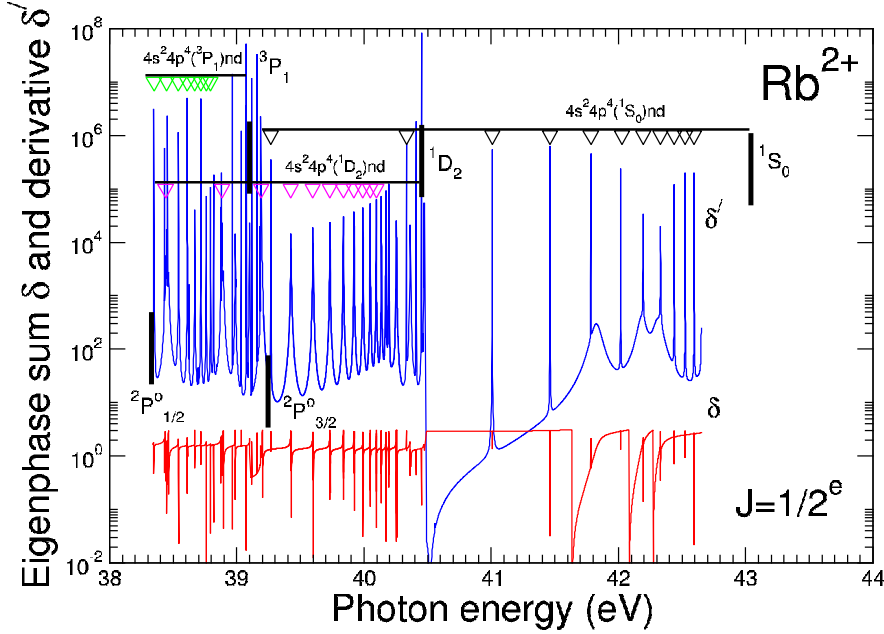


Figure 2. (Colour online) Eigenphase sum (δ , solid red line) and its derivative (δ' , solid blue line) for the $J=1/2$ even scattering symmetry in the energy region 38 - 44 eV from the DARC photoionization out of the $3d^{10}4s^24p^5\ ^2P^o_{1/2}$ metastable state of the Rb^{2+} ion. The prominent $4s^24p^4nd$ Rydberg Auger series parameters (found in the photoionization cross section) converging to the 3P_1 , 1D_2 and 1S_0 thresholds of the Rb^{3+} ion are tabulated in Table 2, 3 and 4. The inverted triangles are the energy positions of the various Rydberg resonance series. Note, the presence of interloping resonances (assigned to the 1S_0 threshold) perturb the regular Rydberg pattern lying below the 1D_2 threshold. In addition interloping resonances associated with higher lying thresholds perturb the Rydberg resonance series assigned to the 1S_0 threshold.

2.3. Resonances

The multi-channel R -matrix eigenphase derivative (QB) technique [51] as developed by Berrington and co-workers [52–54] was used to locate and determine the resonance positions. The resonance autoionization width Γ can be determined from the inverse of the energy derivative of the eigenphase sum δ [55, 56] at the resonance energy E_r via

$$\Gamma = 2 \left[\frac{d\delta}{dE} \right]_{E=E_r}^{-1} = 2 [\delta']_{E=E_r}^{-1}. \quad (3)$$

The Auger widths of the resonances presented in Table 2 - 4 are determined via this method where the eigenphase sum is obtained from the large-scale multi-channel close-coupling electron scattering from the residual Rb^{3+} ion within the context of the R -matrix method [51].

Fig 2 illustrates the eigenphase sum and its derivative, for the $J = \frac{1}{2}$ scattering symmetry, in the photon energy region 38 eV – 44 eV, where prominent Rydberg series are found in the cross section for photoionization out of the initial metastable $^2P_{1/2}^o$ state of the Rb^{2+} ion. As vividly seen from the behaviour of the eigenphase sum derivative, the presence of interloping Rydberg resonances (associated with the 1S_0 threshold) perturb the regular resonance series and disrupt the regular Rydberg pattern lying below the 1D_2 and 1S_0 thresholds. Such perturbing interlopers affect the widths of the resonances as is evidently seen from the results shown in Tables 2 - 4, and in Fig 3. The QB method is suitable for determining the Auger widths of isolated resonances. We note that more elaborate approaches are used to treat overlapping resonances [57–60]. In general, the eigenphase sum derivative, which is proportional to the trace of the lifetime matrix, is expressible in the energy region of resonance n as

$$d\delta/dE = \sum_n (\Gamma_n/2)/[(E_n - E)^2 + (\Gamma_n/2)^2] + d\delta_b/dE, \quad (4)$$

where $d\delta_b/dE$ is the small background contribution. The multi-channel R -matrix QB method used here, analyzes the eigenphase sum and its derivative to extract the resonance parameters. Results are presented in Table 2 - 4. Overlapping resonances can in principle be analyzed by fitting to this formula; however, when there are multiple overlapping resonances a more comprehensive approach is to examine the eigenvalues of the lifetime matrix, see [58,60] and sec. 3.2.4 of [51]. For the present work the QB approach may be used to locate isolated resonance energies and to highlight interloper effects in the spectra.

We attribute the difference in Auger widths to the different number of coupled channels for the $J = \frac{1}{2}$ and $J = \frac{3}{2}$ scattering symmetries. In addition the presence of overlapping and interloping resonances in the spectra disrupt the Rydberg patterns, which we analyze further in Sec. 3 below.

As shown in Tables 2 - 4, theory and experiment are in harmony for the resonant energies and quantum defects. No measurements are available for the Auger widths due to the limited ALS experimental resolution. We note that all of the Auger widths Γ for these Rydberg series have a natural line width very much less than 10 meV. In fact the bulk of them are less than 1 meV. Measurement of such narrow line widths are beyond the present capabilities of the ALS experimental resolution of 13.5 ± 2.5 meV.

An additional check on the theoretical data was carried out by calculating the integrated continuum oscillator strength f from the experimental cross sections over the energy grid $[E_1, E_2]$, where E_1 is the minimum experimental energy (37.31 eV) and E_2 is the maximum experimental energy (44.08 eV), using [61–63],

$$f = 9.1075 \times 10^{-3} \int_{E_1}^{E_2} \sigma(h\nu) dh\nu \quad (5)$$

Evaluating the continuum oscillator strength f for the ALS cross section measurements yielded a value of 0.294 ± 0.060 , where we have estimated an error of 20% from the ALS absolute cross sections values [27]. Evaluation of Eq. (5) for the theoretical Dirac R -matrix cross sections gave a value of 0.420 for the statistical average of the $3d^{10}4s^24p^5\ ^2P_{3/2}^o$ ground state and the $3d^{10}4s^24p^5\ ^2P_{1/2}^o$ metastable state. This value is about 19% outside the experimental error bar. The difference we attribute to the theoretical cross section being larger than experiment in the photon energy range 41.4

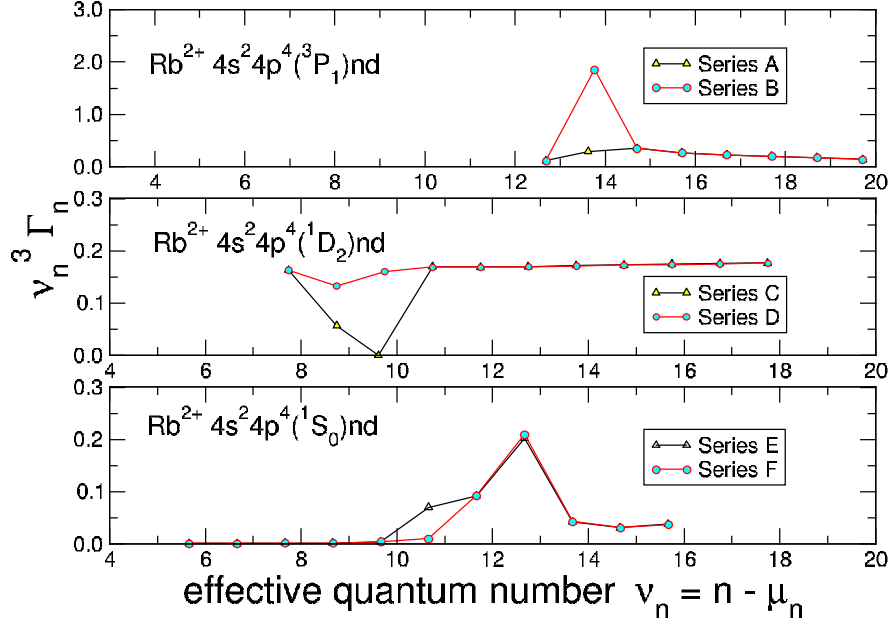


Figure 3. (Colour online) The quantity $\nu_n^3 \Gamma_n$ versus the effective quantum number $\nu_n = n - \mu_n$ for each of the six series, A - F, found in the spectrum. The triangles are for the initial $J = \frac{1}{2}$ state and the corresponding circles are for the initial $J = \frac{3}{2}$ state. The top panel are the $4s^2 4p^4(^3P_1) nd$ series going to the 3P_1 threshold, the middle panel the $4s^2 4p^4(^1D_2) nd$ series going to the 1D_2 threshold, and the bottom panel the $4s^2 4p^4(^1S_0) nd$ series going to the 1S_0 threshold of the Rb^{3+} ion.

- 44 eV, as clearly illustrated in Fig 1. We note that the Breit-Pauli cross section calculations reported in the work of Macaluso and co-workers [27] lie consistently higher than experiment in this same photon energy range. However, in their work Macaluso and co-workers [27] did not report a value for the continuum oscillator strength f . Experimentally, corrections for higher order radiation effects [64] on the cross sections, or methods for piecing together all the various high resolution scans to make a complete spectra (see [65,66]), might also be important. However, in their work Macaluso and co-workers [27] point out that higher order radiation effects are negligible above 40 eV in their Rb^{2+} experiment contributing less than 1% correction.

3. Results and Discussion

As discussed above, the eigenphase sum derivative was used to extract the resonance parameters. The resonance series identification can be made from Rydberg's formula (see, for example, [67]) along with the NIST tabulations [49]. The energy position ϵ_{ν_n}

of a resonance can be obtained via,

$$\epsilon_{\nu_n} = \epsilon_{\infty} - \frac{\mathcal{Z}^2}{\nu_n^2}, \quad (6)$$

with \mathcal{Z} the charge of the core (in the present case $\mathcal{Z} = 3$) and the effective quantum number $\nu_n = n - \mu_n$, ϵ_{∞} is the Rydberg series limit, n is the principal quantum number and μ_n the quantum defect.

Table 2 presents the Auger energies and quantum defects for the Rydberg series found in the $J = \frac{1}{2}$ and $J = \frac{3}{2}$ scattering symmetries, from the DARC 687-level calculations, and compares them with the measurements from the ALS. The parameters are shown for the $4s^24p^4(^3P_1)$ nd series converging to the 3P_1 threshold of the Rb^{3+} ion, where the initial state is the $4s^24p^5(^2P^{\circ}_{3/2})$ ground state and the $4s^24p^5(^2P^{\circ}_{1/2})$ metastable state. In Table 3 results are shown for the $4s^24p^4(^1D_2)$ nd series converging to the 1D_2 threshold and in Table 4 results are presented for the $4s^24p^4(^1S_0)$ nd series converging to the 1S_0 threshold of the Rb^{3+} ion.

First and foremost from Table 2 - 4 the widths of the various Rydberg resonance series are perturbed by the presence of interlopers. For regular Rydberg series then $\nu_n^3\Gamma_n$ should go smoothly to a constant as $\nu_n \rightarrow \infty$. Note, from the results for the Auger widths presented in Table 2 - 4, and in Fig 3, irregular behaviour is seen. For the Auger widths presented in Tables 2 - 4 the disruption of the smooth decay of the resonance width Γ_n along the Rydberg series is due to the presence of interlopers. This is evident for the resonance series associated with the 3P_1 , 1D_2 and 1S_0 , Rb^{3+} thresholds, as illustrated in Fig 2, and in Fig 3. For example, the Auger widths for the $n = 11, 12, 13,$ and 14 members of the $4s^24p^4(^1S_0)$ nd series, $J = \frac{1}{2}$ scattering symmetry, in Table 4, clearly illustrate this disruption effect.

4. Summary and Conclusions

We have carried out large-scale PI cross section calculations using the parallel version of the DARC codes. Our statistically averaged cross sections for the ground and metastable states show excellent agreement with the recent measurements from the ALS [27] radiation facility from thresholds to about 41.4 eV. The present theoretical cross sections in the photon region 41.4 - 44 eV are on average about 20% higher than experiment, but they are consistent with previous Breit-Pauli calculations performed on this complex [27]. An analysis of the Auger Rydberg resonances series using the eigenphase sum derivative approach show excellent agreement with previous results within the experimental resolution [27, 28]. Comparison between theory and experiment for resonance energies and quantum defects in Tables 2 - 4, provide further confidence in our theoretical data for applications in astrophysics. Numerical values of the DARC PI cross sections are available on request from the authors.

Table 2. Resonance energies E_n and quantum defects μ_n of the $4s^24p^4(^3P_1) nd$ Rydberg series (from the 687-level DARC calculations), compared with the ALS measurements, for the $J = \frac{1}{2}$ and $J = \frac{3}{2}$ scattering symmetries, converging to the $Rb^{3+}(3d^{10}4s^24p^4 \ ^3P_1)$ threshold originating from the Rb^{2+} ground $4s^24p^5 \ ^2P^o_{3/2}$ and metastable state $4s^24p^5 \ ^2P^o_{1/2}$.

Series A		$4s^24p^5(^2P^o_{1/2})$ initial state		$4s^24p^5(^2P^o_{1/2})$ initial state	
		Experiment (ALS)		Theory (DARC)	
n	$E_n(\text{eV})$	μ_n	$E_n(\text{eV})$	μ_n	$\Gamma_n(\text{meV})$
13	38.352	0.28	38.348	0.31	0.8
14	38.459	0.28	38.449	0.31	1.6
15	38.544	0.28	38.543	0.30	1.5
16	38.614	0.28	38.612	0.30	0.9
17	38.671	0.28	38.670	0.30	0.7
18	38.719	0.28	38.718	0.31	0.5
19	38.760	0.28	38.759	0.30	0.4
20	38.794	0.28	38.794	0.28	0.3
–	–	–	–	–	–
\vdots	\vdots	\vdots	\vdots	\vdots	\vdots
∞	39.109	–	39.109	–	–

Series B		$4s^24p^5(^2P^o_{3/2})$ initial state		$4s^24p^5(^2P^o_{3/2})$ initial state	
		Experiment (ALS)		Theory (DARC)	
n	$E_n(\text{eV})$	μ_n	$E_n(\text{eV})$	μ_n	$\Gamma_n(\text{meV})$
13	39.268	0.27	39.263	0.31	0.8
14	39.374	0.27	39.379	0.32	9.7
15	39.459	0.27	39.457	0.32	1.5
16	39.528	0.27	39.526	0.30	0.9
17	39.586	0.27	39.584	0.30	0.7
18	39.634	0.27	39.632	0.32	0.5
19	39.674	0.27	39.673	0.30	0.4
20	39.709	0.27	39.707	0.30	0.3
–	–	–	–	–	–
\vdots	\vdots	\vdots	\vdots	\vdots	\vdots
∞	40.023	–	40.023	–	–

Table 3. Resonance energies E_n and quantum defects μ_n of the $4s^24p^4(^1D_2) nd$ Rydberg series (from the 687-level DARC calculations), compared with the ALS measurements, for the $J = \frac{1}{2}$ and $J = \frac{3}{2}$ scattering symmetries, converging to the $Rb^{3+}(3d^{10}4s^24p^4\ ^1D_2)$ threshold originating from the Rb^{2+} ground $4s^24p^5\ ^2P^{\circ}_{3/2}$ and metastable state $4s^24p^5\ ^2P^{\circ}_{1/2}$.

Series C		$4s^24p^5(^2P^{\circ}_{1/2})$ initial state		$4s^24p^5(^2P^{\circ}_{1/2})$ initial state	
		Experiment (ALS)		Theory (DARC)	
n	$E_n(\text{eV})$	μ_n	$E_n(\text{eV})$	μ_n	Γ_n (meV)
8	38.446	0.25	38.440	0.26	4.8
9	38.885	0.25	38.884	0.25	1.2
10	39.196	0.25	39.192	0.26	10^{-3}
11	39.425	0.25	39.424	0.26	1.8
12	39.598	0.25	39.597	0.26	1.4
13	38.731	0.25	39.731	0.26	1.1
14	39.837	0.25	39.837	0.26	0.9
15	39.922	0.25	39.222	0.26	0.7
16	39.991	0.25	39.991	0.26	0.6
17	40.048	0.25	40.048	0.26	0.5
18	40.096	0.25	40.096	0.26	0.4
–	–	–	–	–	–
\vdots	\vdots	\vdots	\vdots	\vdots	\vdots
∞	40.485	–	40.485	–	–
Series D		$4s^24p^5(^2P^{\circ}_{3/2})$ initial state		$4s^24p^5(^2P^{\circ}_{3/2})$ initial state	
		Experiment (ALS)		Theory (DARC)	
n	$E_n(\text{eV})$	μ_n	$E_n(\text{eV})$	μ_n	Γ_n (meV)
8	39.347	0.28	39.355	0.26	4.8
9	39.790	0.28	39.797	0.26	2.7
10	40.104	0.28	40.109	0.26	2.4
11	40.334	0.28	40.339	0.26	1.9
12	40.508	0.28	40.511	0.26	1.4
13	40.643	0.28	40.645	0.26	1.1
14	40.749	0.28	40.751	0.26	0.9
15	40.834	0.28	40.836	0.26	0.7
16	40.904	0.28	40.905	0.26	0.6
17	40.961	0.28	40.962	0.26	0.5
18	41.009	0.28	41.010	0.26	0.4
–	–	–	–	–	–
–	–	–	–	–	–
\vdots	\vdots	\vdots	\vdots	\vdots	\vdots
∞	41.399	–	41.399	–	–

Table 4. Resonance energies E_n and quantum defects μ_n of the $4s^24p^4(^1S_0) nd$ Rydberg series (from the 687-level DARC calculations), compared with the ALS measurements, for the $J = \frac{1}{2}$ and $J = \frac{3}{2}$ scattering symmetries, converging to the $Rb^{3+}(3d^{10}4s^24p^4 \ ^1S_0)$ threshold originating from the Rb^{2+} ground $4s^24p^5 \ ^2P^{\circ}_{3/2}$ and metastable state $4s^24p^5 \ ^2P^{\circ}_{1/2}$.

Series E		$4s^24p^5(^2P^{\circ}_{1/2})$ initial state		$4s^24p^5(^2P^{\circ}_{1/2})$ initial state	
		Experiment (ALS)		Theory (DARC)	
n	E_n (eV)	μ_n	E_n (eV)	μ_n	Γ_n (meV)
6	39.332	0.30	39.267	0.34	0.1
7	40.373	0.30	40.333	0.34	0.1
8	41.037	0.30	41.008	0.34	0.1
9	41.484	0.30	41.462	0.34	0.1
10	41.802	0.30	41.782	0.34	0.1
11	42.034	0.30	42.026	0.34	0.8
12	42.209	0.30	42.194	0.34	1.4
13	42.345	0.30	42.331	0.34	0.2
14	42.451	0.30	42.438	0.34	0.2
15	42.537	0.30	42.524	0.34	0.1
16	42.607	0.30	42.595	0.34	0.1
–	–	–	–	–	–
\vdots	\vdots	\vdots	\vdots	\vdots	\vdots
∞	43.094	–	43.094	–	–

Series F		$4s^24p^5(^2P^{\circ}_{3/2})$ initial state		$4s^24p^5(^2P^{\circ}_{3/2})$ initial state	
		Experiment (ALS)		Theory (DARC)	
n	E_n (eV)	μ_n	E_n (eV)	μ_n	Γ_n (meV)
6	40.242	0.31	40.182	0.34	0.1
7	41.286	0.31	41.248	0.34	0.1
8	41.950	0.31	41.922	0.34	0.1
9	42.398	0.31	42.376	0.34	0.1
10	42.715	0.31	42.697	0.34	0.1
11	42.947	0.31	42.931	0.34	0.1
12	43.127	0.31	43.108	0.34	1.0
13	43.258	0.31	43.245	0.34	1.4
14	43.365	0.31	43.353	0.34	0.2
15	43.451	0.31	43.439	0.34	0.2
16	43.521	0.31	43.509	0.34	0.1
–	–	–	–	–	–
\vdots	\vdots	\vdots	\vdots	\vdots	\vdots
∞	44.088	–	44.088	–	–

Acknowledgments

B M McLaughlin acknowledges support by the National Science Foundation (USA) through a grant to ITAMP at the Harvard-Smithsonian Center for Astrophysics under the visitors program, the University of Georgia at Athens for the award of an adjunct professorship and Queen's University Belfast for a visiting research fellowship (VRF). Professor David Macaluso is thanked for the provision of the published ALS data in numerical format and Captain Thomas J. Lavery USN Ret. for his constructive comments that enhanced the quality of this manuscript. We dedicate this work to the staff of the cardiac unit at the INOVA hospital in Fairfax, Virginia, USA, who graciously provided facilities for the completion of this manuscript. The authors acknowledge this research used grants of computing time at the National Energy Research Scientific Computing Centre (NERSC), which is supported by the Office of Science of the U.S. Department of Energy (DOE) under Contract No. DE-AC02-05CH11231. The authors gratefully acknowledge the Gauss Centre for Supercomputing e.V. (www.gauss-centre.eu) for funding this project by providing computing time on the GCS Supercomputer HAZEL HEN at Höchstleistungsrechenzentrum Stuttgart (www.hlr.de). ITAMP is supported in part by NSF Grant No. PHY-1607396.

References

- [1] Pequignot D and Baluteau J P 1994 *Astron. & Astrophys.* **283** 593–625
- [2] Sharpee B, Zhang Y, Williams R, Pellegrini E, Cavagnolo K, Baldwin J A, Phillips M and Liu X W 2007 *Astrophys. J.* **659** 1265–1290 (*Preprint* [astro-ph/0612101](#))
- [3] Sterling N C and Dinerstein H L 2008 *Astrophys. J. Suppl.* **174** 154
- [4] Otsuka M and Tajitsu A 2013 *Astrophys. J.* **778** 146 (*Preprint* [1310.1151](#))
- [5] García-Rojas J, Madonna S, Luridiana V, Sterling N C, Morisset C, Delgado-Inglada G and Toribio San Cipriano L 2015 *Mon. Not. Roy. Astro. Soc.* **452** 2606–2640 (*Preprint* [1506.07079](#))
- [6] Sterling N C, Dinerstein H L, Kaplan K F and Bautista M A 2016 *Astrophys. J.* **819** L9 (*Preprint* [1602.03188](#))
- [7] Langanke K and Wiescher M 2001 *Rep. Prog. Phys.* **64** 1657
- [8] Kwitter K B, Méndez R H, Peña M, Stanghellini L, Corradi R L M, De Marco O, Fang X, Henry R B C, Karakas A I, Liu X W, López J A, Manchado A and Parker Q A 2014 *Rev. Mex. Astron. Astro.* **50** 203–223 (*Preprint* [1403.2246](#))
- [9] Sterling N C, Porter R L and Dinerstein H L 2015 *Astron. Astrophys. Suppl.* **218** 25 (*Preprint* [1505.01162](#))
- [10] Stasińska G 2017 *Can. J. Phys.* **95** 821–824
- [11] Walker K M, Federman S R, Knauth D C and Lambert D L 2009 *Astrophys. J.* **706** 614–622
- [12] Cardelli J A, Federman S R, Lambert D L and Theodosiou C E 1993 *Astrophys. J.* **416** 41
- [13] Smith V V and Lambert D L 2015 *Astrophys. J. Suppl.* **72** 387
- [14] Wallerstein G, et al 1997 *Rev. Mod. Phys.* **69** 995
- [15] Busso M, Gallino R and Wasserburg G J 1999 *Ann. Rev. Astron. & Astrophys.* **37** 239
- [16] Travaglio C, Gallino R, Arnone E, Cowan J J, Jordan F and Sneden C 2004 *Astrophys. J.* **60** 186
- [17] Herwig F 2005 *Ann. Rev. Astron. & Astrophys.* **43** 435
- [18] Sneden C et al 2008 *Ann. Rev. Astron. & Astrophys.* **46** 241
- [19] Sansonetti J E 2006 *J. Phys. Chem. Ref. Data* **35** 301–421
- [20] Persson W and Wahlström C G 1985 *Physica Scripta* **31** 487–505
- [21] Mueller A, Macaluso D A, Sterling N, Juarez A, Dumitriu I, Bilodeau R, Red E, Hardy D and Aguilar A 2013 *Bull. Am. Phys. Soc.* **58**(6) 178
- [22] Kilbane D, Folkman F, Bizau J M, Banahan C, Scully S, Kjeldsen H, van Kampen P, Mansfield M W D, Costello J T and B W J 2007 *Phys. Rev. A* **75** 032711
- [23] Neogi A, Kennedy E T, Mosnier J P, van Kampen P, Costello J T O'Sullivan G, Mansfield M W D, Demekhin P V, Lagutin B M and Sukhorukov V L 2003 *Phys. Rev. A* **67** 042707

- [24] McLaughlin B M and Babb J F 2019 *Mon. Not. Roy. Astro. Soc.* **486** 245
- [25] Demekhin P V, Petrov I D, Lagutin B M, Sukhorukov V L, Neogi A, Yeates P, Kennedy E T, Mansfield M W D and Costello J T 2007 *Opt. Spectrosc.* **102** 149
- [26] Luridiana V, Morisset C and Shaw R A 2015 *Astron. & Astrophys.* **573** A42 URL <https://doi.org/10.1051/0004-6361/201323152>
- [27] Macaluso D A, Bogolub K, Johnson A, Aguilar A, Kilcoyne A L D, Bilodeau R C, Bautista M, Kerlin A B and Sterling N C 2016 *J. Phys. B: At. Mol. Opt. Phys.* **49** 235002
- [28] Macaluso D A, Bogolub K, Johnson A, Aguilar A, Kilcoyne A L D, Bilodeau R C, Bautista M, Kerlin A B and Sterling N C 2017 *J. Phys. B: At. Mol. Opt. Phys.* **50** 119501
- [29] Dyall K G, Johnson C T, Grant I P, Parpia F, and Plummer E P 1989 *Comput. Phys. Commun.* **55** 425
- [30] Parpia F, Froese-Fisher C and Grant I P 2006 *Comput. Phys. Commun.* **94** 249
- [31] Grant I P 2007 *Relativistic Quantum Theory of Atoms and Molecules: Theory and Computation* (New York, USA: Springer)
- [32] Ballance C P and Griffin D C 2006 *J. Phys. B: At. Mol. Opt. Phys.* **39** 3617
- [33] Fivet V, Bautista M A and Ballance C P 2012 *J. Phys. B: At. Mol. Opt. Phys.* **45** 035201
- [34] Norrington P H and Grant I P 1987 *J. Phys. B: At. Mol. Phys.* **20** 4869
- [35] Wijesundera W P, Parpia F A, Grant I P and Norrington P H 1991 *J. Phys. B: At. Mol. Phys.* **24** 1803
- [36] Ballance C P 2018 DARC codes website URL <http://connorb.freeshell.org>
- [37] McLaughlin B M and Ballance C P 2012 *J. Phys. B: At. Mol. Opt. Phys.* **45** 085701
- [38] McLaughlin B M and Ballance C P 2012 *J. Phys. B: At. Mol. Opt. Phys.* **45** 095202
- [39] McLaughlin B M, Ballance C P 2015 Petascale computations for large-scale atomic and molecular collisions *Sustained Simulated Performance 2014*, ed Resch M M, Kovalenko Y, Fotch E, Bez W and Kobaysah H (Berlin, Germany: Springer) pp 173–190
- [40] McLaughlin B M, Ballance C P, Pindzola M S and Müller A 2015 PAMOP: petascale atomic, molecular and optical collisions *High Performance Computing in Science and Engineering'14* ed Nagel W E, Kröner D H and Resch M M (Berlin, Germany: Springer) pp 23–40
- [41] McLaughlin B M, Ballance C P, Pindzola M S, Schippers S and Müller A 2016 PAMOP project : Petaflop computations in support of experiments *High Performance Computing in Science and Engineering'15* ed Nagel W E, Kröner D H and Resch M M (Berlin, Germany: Springer) pp 51–74
- [42] McLaughlin B M, Ballance C P, Pindzola M S, Stancil P C, Schippers S and Müller A 2017 PAMOP project : Petaflop computations in support of experiments *High Performance Computing in Science and Engineering'16* ed Nagel WE, Kröner D H and Resch M M (Berlin, Germany: Springer) pp 33–48
- [43] McLaughlin B M, Ballance C P, Pindzola M S, Stancil P C, Babb J F, Schippers S and Müller A 2018 PAMOP: Large-scale calculations supporting experiments and astrophysical applications *High Performance Computing in Science and Engineering'17* ed Nagel W E, Kröner D H and Resch M M (Berlin, Germany: Springer) pp 37–59
- [44] McLaughlin B M, Ballance C P, Pindzola M S, Stancil P C, Babb J F, Schippers S and Müller A 2019 PAMOP2: Towards Exascale Computations Supporting Experiments and Astrophysics *High Performance Computing in Science and Engineering'18* ed Nagel W E, Kröner D H and Resch, M M (Berlin, Germany: Springer) pp 37–59
- [45] Müller A, Schippers S, Hellhund J, Kilcoyne A L D, Phaneuf R A and McLaughlin B M 2017 *J. Phys. B: At. Mol. Opt. Phys.* **50** 085007
- [46] Smyth R T, Johnson C A, Ennis D A, Loch S D, Ramsbottom C A and Ballance C P 2017 *Phys. Rev A* **96** 042713
- [47] Müller A, Schippers S, Phaneuf R P, Covington A M, Aguilar A, Hinojosa G, Bozeck J, Sant'Anna M M, Schlachter A S, Cisneros C and McLaughlin B M 2017 *J. Phys. B: At. Mol. Opt. Phys.* **50** 205001
- [48] Smyth R T, Ramsbottom C A and Ballance C P 2018 *Galaxies* **6** 87
- [49] Kramida A E, Ralchenko Y and Reader J and NIST ASD Team 2018 NIST Atomic Spectra Database (version 5.6.1) National Institute of Standards, Technology, Gaithersburg, MD, USA URL <http://physics.nist.gov/>
- [50] Rohl J W 1994 *Modern Physics from A to Z* (New York, USA: Wiley)
- [51] Burke P G 2011 *R-Matrix Theory of Atomic Collisions: Application to Atomic, Molecular and Optical Processes* (New York, USA: Springer)
- [52] Quigley L and Berrington K A 1996 *J. Phys. B: At. Mol. Phys.* **29** 4529
- [53] Quigley L, Berrington K A and Pelan J 1998 *Comput. Phys. Commun.* **114** 225
- [54] Ballance C P, Berrington K A and McLaughlin B M 1999 *Phys. Rev. A* **60** R4217

- [55] Smith F T 1960 *Phys. Rev.* **114** 349
- [56] Forrey R C, Balakrishnan N, Kharchenko V and Dalgarno A 1998 *Phys. Rev. A* **58** R2645
- [57] Igarashi A and Shimamura I 2004 *J. Phys. B: At. Mol. Opt. Phys.* **37** 4221
- [58] Shimamura I, McCann J F and Igarashi A 2006 *J. Phys. B: At. Mol. Opt. Phys.* **39** 1847
- [59] Aiba K, Igarashi A and Shimamura I 2007 *J. Phys. B: At. Mol. Opt. Phys.* **40** F9
- [60] Shimamura I 2012 Quasi-Bound States of Electronic and Positronic Few-Body Systems: Analysis of Multi-Channel Scattering Information *Unstable States in the Continuous Spectra Part II: Interpretation, Theory and Applications (Advanced Series in Quantum Chemistry vol 63)* ed Nicolaiades C A and Brändas E J (Waltham, Massachusetts, USA: Academic Press) p 165 1st ed
- [61] Shore B W 1967 *Rev. Mod. Phys.* **39** 439
- [62] Fano U and Cooper J W 1967 *Rev. Mod. Phys.* **40** 441
- [63] Berkowitz J 1979 *Photoabsorption, Photoionization and Photoelectron Spectroscopy* (New York, USA: Academic Press)
- [64] Müller A, Schippers S, Hellhund J, Holste K, Kilcoyne A L D, Phaneuf R, Ballance C P and McLaughlin B M 2017 *J. Phys. B: At. Mol. Opt. Phys.* **48** 235203
- [65] Müller A, Phaneuf R, Aguilar A, Gharaibeh, Schlachter A S, Alvarez I, Cisneros C, Hinojosa G and McLaughlin B M 2002 *J. Phys. B: At. Mol. Opt. Phys.* **35** L137
- [66] Schippers S, Müller A, McLaughlin B M, Aguilar A, Cisneros C, Emmons E D, Gharaibeh M F and Phaneuf R 2003 *J. Phys. B: At. Mol. Opt. Phys.* **36** 3371
- [67] Seaton M J 1983 *Rep. Prog. Phys.* **46** 161